Surfaces decorated with enantiomorphically pure polymer nanohelices via hierarchical chirality transfer across multiple length scales

Divya Varadharajan, Karthik Nayani, Christoph Zippel, Eduard Spuling, Kenneth C. Cheng, Swetha Sarangarajan, Sangchul Roh, John Kim, Vanessa Trouillet, Stefan Bräse, Nicholas L. Abbott, Joerg Lahann**

D. Varadharajan, S. Sarangarajan, J. Lahann*

Institut für Funktionelle Grenzflächen (IFG), Karlsruhe Institute of Technology (KIT) 76344, Eggenstein-Leopoldshafen, Germany

K. Nayani

Martin Department of Chemical Engineering, University of Arkansas, 72701-1201, Fayetteville, AR, USA

C. Zippel, E. Spuling, S. Bräse

Institut für Organische Chemie Karlsruher Institut für Technologie (KIT), 76131, Karlsruhe, Germany

K.C. Cheng, J. Kim, J. Lahann*

Biointerfaces Institute, University of Michigan, 48105, Ann Arbor, MI, USA

Department of Materials Science and Engineering, University of Michigan, 48109-2102, Ann Arbor, MI, USA

S. Roh, N.L. Abbott*

Smith School of Chemical and Biomolecular Engineering, Cornell University, 14853, Ithaca, NY, USA

V.Trouillet

Institut fuer Angewandte Materialien (IAM-ESS) and Karlsruhe Nano Micro Facility KNMF), 76344, Eggenstein-Leopoldshafen, Germany

S. Bräse

This is the author manuscript accepted for publication and has undergone full peer review but has not been through the copyediting, typesetting, pagination and proofreading process, which may lead to differences between this version and the Version of Record. Please cite this article as doi: 10.1002/adma.202108386.

Institute of Biological and Chemical Systems (IBCS-FMS), Karlsruhe Institute of Technology (KIT), 76344, Eggenstein-Leopoldshafen, Germany

E-mail: lahann@umich.edu; nla34@cornell.edu

Keywords: nanohelix, chirality transfer, paracyclophane, liquid crystal, template, chemical vapor deposition, polymerisation

Abstract: Mesoscale chiral materials have been prepared by lithographic methods, assembly of chiral building blocks, and through syntheses in the presence of polarised light. Typically, these processes result in micrometer-sized structures, require complex top-down manipulation, or rely on tedious asymmetric separation. We discovered that the chemical vapor deposition of chiral precursors into supported films of liquid crystals (LCs) results in superhierarchical arrangements of enantiomorphically pure nanofibers. Depending on the molecular chirality of the 1-hydroxyethyl [2.2]paracyclophane precursor, extended arrays of enantiomorphic nanohelices are formed from achiral nematic templates. Arrays of chiral nanohelices extend over hundreds of microns and consistently display enantiomorphic micropatterns. The pitch of individual nanohelices depend on the enantiomeric excess and the purity of the chiral precursor, consistent with the theoretical model of a doubly-twisted LC director configuration. During CVD of chiral precursors into cholesteric LC films, aspects of molecular and mesoscale asymmetry combine constructively to form regularly twisted nanohelices. Enantiomorphic surfaces permit the tailoring of a wide range of functional properties, such as the asymmetric induction of weak chiral systems.

1. Introduction

Surfaces with mesoscale chirality are central to a range of emerging fields, including photonics, electronics,[1–3] chiral recognition,[4,5] biocompatible cell scaffolds,[6] or asymmetric crystallization.[7,8] Chirality, a direct consequence of mirror-image asymmetry, is one of the most fundamental structural elements in nature, enabling functions at molecular (e.g., amino acids), macromolecular (e.g., DNA), mesoscopic (e.g., collagen triple helix), and macroscopic (e.g., *Vitis vinifera*) scales. In nature, chiral precursors are assembled into macromolecular units and further into mesoscale structures, with the

successive transfer of chiral information at each stage.[9] While nature's approach to homochirality has been a source of inspiration for chemists and materials scientists, the preparation of enantiomorphically pure materials has been synthetically challenging and generally requires asymmetric separation after assembly. Helical structures are among the most widely evaluated chiral materials that have been fabricated by supramolecular self-assembly of inorganic or organic chiral building blocks[10] as well as lithographic methods, such as direct laser writing[11–13]. Chiral surfaces based on arrays of nanohelices up to 50 nm in diameter have been prepared using focused ion-beam deposition of metal-organic precursors. However, this technique is restricted to metals such as platinum, tungsten, and gold and is additionally limited in resolution due to the beam properties.[14–17] Emulating nature's multiscale chirality transfer approach, we pursued the LC-templated CVD polymerisation of chiral precursors to fabricate enantiomorphic surfaces comprised of arrays of nanohelices. Our approach builds upon recent findings that CVD of [2.2]paracylcophanes into supported LC films gives rise to extended arrays of well-defined nanofibers.[18]

2. Results and Discussion

2.1. Formation of chirality-defined superhierarchical arrays of nanohelices

In contrast to previous work by us and others,[18,19] the chiral information is directly encoded in the precursor, rather than the templating LC medium, which remains achiral. We previously[18] reported the formation of nanofibers by CVD polymerisation of achiral [2.2] paracyclophane precursors into achiral and chiral nematic LC phases emphasising the role of the template in dictating the morphology of the nanofibers. This work builds upon earlier work by our group demonstrating the use of CVD polymerization to create functional polymer coatings on a wide range of substrates.[20-24] One of the key differences herein is our focus on the influence of the chemical nature of the precursors that allow for the fabrication of nanohelices with tunable properties. We demonstrate that templated CVD polymerisation of chiral precursors results in superhierarchical arrays of nanohelices with defined chirality across multiple length scales. Consistent with this approach, CVD polymerisation of two chiral precursors (Sp,S)-1-(4-[2.2]paracyclophanyl)ethanol (**1S**) and (Sp,R)-1-(4-[2.2]paracyclophanyl)ethanol (**1R**) into a nematic LC film (E7) resulted in regular arrays of nanohelices (Figure 1A). A detailed explanation for the preparation of the substrates as well as the CVD polymerisation process has been described in the experimental section. Briefly, a pre-weighed amount

(4 mg) of the precursor **1S** or **1R** was polymerised by CVD polymerisation into a 10-12 µm thick nematic LC template E7 film pre-loaded into TEM grid wells placed on a homeotropically aligned glass substrate. The sublimation of the precursor was maintained at a constant rate of 0.2-0.4 Å/sec throughout the CVD polymerisation process to ensure a low and uniform influx of the precursor radicals into the LC template. After complete sublimation of the precursor, the CVD polymerization was terminated, the LC phase removed and the nanohelices were harvested for further characterization. The chiral precursors **1S** and **1R** were prepared by asymmetric synthesis of from (Sp)-4-formyl[2.2]paracyclophane using methyl lithium and chiral chromatography resulting in homochiral precursors (enantiomeric excess of >98% as described in the supplementary text). The ^{1}H and ^{13}C NMR spectra (Figure S1 and S2) confirm the predicted chemical structure of both precursors. During templated CVD polymerisation, E7 was chosen as the nematic medium,[25] because it has a wide nematic temperature range and is highly birefringent.

After the polymerisation of 1S and 1R into E7 to obtain the nanohelices as shown in Figure 1, complete removal of the templating LC phase was confirmed by internal reflection-absorption spectroscopy (IRRAS, Figure S3, top) and X-ray photoelectron spectroscopy (XPS, Figure S3, bottom) based on the absence of -CN bands and N_{1s} signals in the respective spectra of the nanohelices. Dependent on the molecular handedness of the precursor, nanohelices with exclusively counter-clockwise (CCW, **2S** or clockwise (CW, **2R**) twists were observed (Figure 1, B-C) as confirmed by SEM analysis of an area of 250 µm^2. In contrast, templated CVD polymerisation of the achiral precursor **1A** under otherwise identical conditions resulted in straight nanofibers rather than nanohelices (Figure 1D). Replacing the chiral alcohol group in **1S** and **1R** with alternate side groups, such as methoxyethane (PCP(CHOMeMe)), 2-methylpropan-1-ol (PCP(CHOHiPr)), or phenylmethanol (PCP(CHOHPh)) did not result in the formation of nanohelices (Figure S4). This indicates that H-bonding involving the hydroxyl side group may contribute to the formation of nanohelices. Moreover, the incorporation of bulkier side groups appears to prevent the formation of nanohelices, presumably, due to steric effects.

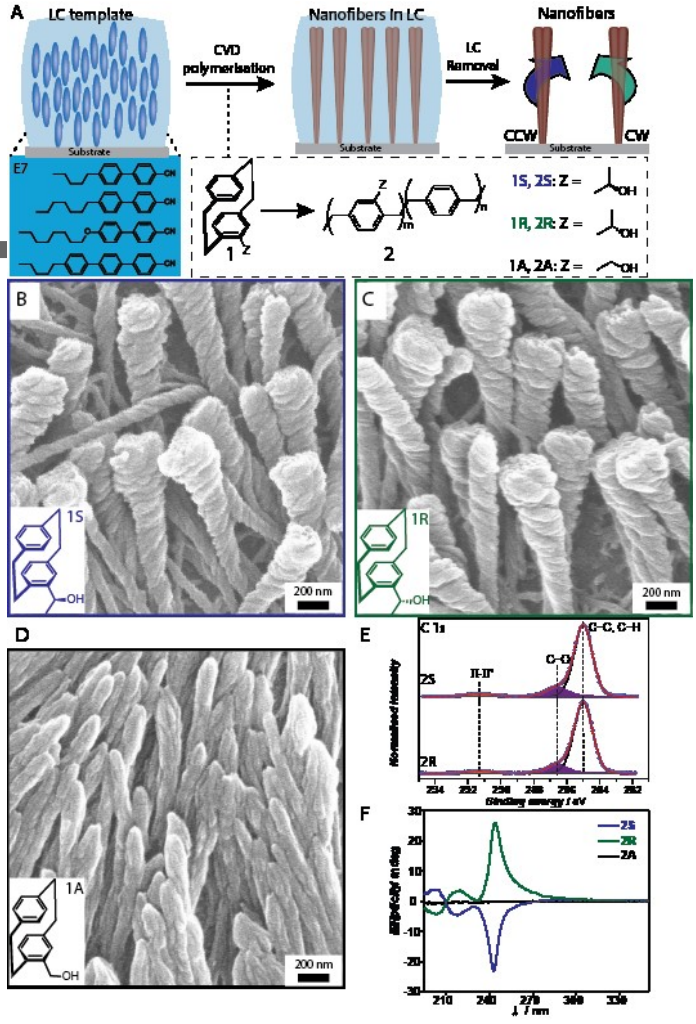

Figure 1: Templated synthesis of polymer nanohelices via CVD polymerisation into a nematic LC film. (A) Schematic representation of nanohelices 2S and 2R templated into the nematic E7 phase. Inset: Chemical representation of CVD polymerisation of chiral and achiral precursors. (B-D) SEM images of nanohelices 2S and 2R and achiral nanofibers 2A prepared by CVD polymerisation of 1S (B), 1R (C), and 1A (D), respectively (The LC is homeotropically anchored on a surface before polymerisation and was removed prior to SEM). (E) High-resolution C1s XPS spectra of 2S and 2R confirming identical chemical composition for nanohelices with opposite handedness; these spectra are identical to the achiral nanofibers 2A shown in Figure S5 ([18]) (F) Circular dichroism (CD) spectra of nanohelices 2S (blue) and 2R (green) and achiral nanofibers 2A (black).

When comparing surfaces decorated with arrays of **2S** and **2R** with each other and to that of the achiral nanofibers **2A**, identical chemical compositions were observed by XPS (Figure 1E and Figure S5) and IR spectroscopy (Figure S3, top). The chemical compositions were also comparable to the respective polymer films prepared by CVD polymerisation of **1S** and **1R** in the absence of a templating LC medium (Figure S6). The chemical equivalence of both **2S** and **2R** surfaces, as well as chiral and achiral surfaces, is further corroborated by close-to-identical intensity ratios for (C-O)/[(C-C,C-H) + (π-π*)]. After removing the support, circular dichroism (CD) spectroscopy of nanohelical dispersions of either **2S** or **2R** in methanol indicates mirrored signals at 242 nm of similar magnitude and opposite cotton effects (Figure 1F, blue and green curves). The mirror image signals imply that the chirality of the chiral inducers, i.e., **1S** and **1R** determines the helical sense depends on the polymer assembly in the nanohelices. The positive and negative bisignate Cotton effects indicate right- and left-handed screw structures, respectively, according to the exciton coupling theory.[26] Hence, **2S** showing a negative bisignate Cotton effect, has a left-handed π-stacked structure with M-helicity, while **2R** with a positive bisignate Cotton effect features a right-handed structure with P-helicity. For comparison, the CD spectrum of disperse on of **2A** did not show any discernible signals (Figure 1F, black).

All nanohelices showed a continuous increase in diameter from approximately 50 nm at the base, corresponding to the approximate diameter of a single nanofiber to about 350 nm at the top. The average nanohelix lengths and widths (measured at full width half maxima) were 3.2 ± 2.2 μm and 184 ± 51 nm for **2R** and 2.7 ± 1.6 μm and 188 ± 53 nm for **2S**. The observed nanohelix lengths were only about one-third of the LC film thickness (10-12 μm) and thus significantly shorter than achiral nanofibers prepared by templated CVD polymerisation.[18] We thus evaluated the contour length of one turn of the nanohelices, $\boldsymbol{L_o}$, as:

$$\boldsymbol{L_o} = \sqrt{\boldsymbol{p}^2 + (2\pi \boldsymbol{R})^2} \qquad (1)$$

where $\boldsymbol{R}$ is the average radius and $\boldsymbol{p}$ is the average pitch of the nanohelices. Here, the total contour length spanned by a filament in a bundle is $\boldsymbol{L_o * n}$, where $\boldsymbol{n}$, the total number of pitch-turns for a filament bundle (Figure S7). We observed a good agreement between the LC films thicknesses used for experiments and the contour length of the fibers as presented in **Table 1**, corroborating previous findings that the thickness of the templating LC constitutes an upper limit for the length of the nanofibers.[18]

Table 1. The contour lengths of individual nanofibers and that of the nanohelices obtained on polymerising 1S and 1R into E7 with varying film thickness.

Monomer	LC film thickness (μm)	Actual length of a nanohelix (μm)	Contour length, single nanohelix (μm)
1S	10	3.22 ± 2.18	9.74 ± 4.63
1R	10	2.65 ± 1.58	8.20 ± 2.89

2.2. Chirality transfer across multiple length scales

2.2.1. Role of stereogenic center in the formation of nanohelices

In principle, the chiral precursors used for templated CVD polymerisation could act as chiral dopants after they enter the LC phase, thereby forming a chiral-nematic LC phase that could act as the template for the CVD polymerisation. To probe this potential mechanism, the nematic LC phase was doped with either 2.28% **1S** (i.e., the dimer) or 5.9% S-DMPE ((1S)-1-(2,5-dimethylphenyl)ethanol, a molecule structurally resembling the chiral monomer unit of polymer **2S**). The amount of dopant used in these studies is comparable to other studies with chiral-nematic LC phases.[27,28] However, neither **1S** nor S-DMPE resulted in the formation of a chiral-nematic phase as shown by the polarized light microscopy (PLM) images shown as inserts in Figure S8. Subsequent CVD polymerisation into the 1S- and S-DMPE-doped LC phases using the achiral precursor **1A** resulted in the formation of nanofibers without any discernable sign of helicity (Figure S8 C,D,G,H). In contrast, CVD polymerisation of the chiral precursor **1S** under otherwise identical conditions resulted in the formation of nanohelices (Figure S8 A,B,E,F). Based on these findings, we concluded that the chiral precursors used for CVD polymerisation were not able to induce the formation of a chiral-nematic LC phase - ruling it out as the origin of the

nanohelices. However, the presence of a stereogenic center in the CVD precursors appeared to be a prerequisite for the templated synthesis of nanohelices. Both of these findings point towards the chirality transfer across the continuum of molecular, macromolecular and microscopic scales.

For enantiomerically pure nanohelices **2S (**Figure 1**)**, the pitch varied between 108 ± 7 nm and 156 ± 10 (100% **1S**). Diluting the chiral content by templated CVD polymerisation of mixtures of **1S** and the achiral **1A** resulted in an increased pitch and the appearance of more loosely wound nanohelices (**Figure 2**A). While the (90% **1S** + 10% **1A**) mixture had a ***p*** value of 160 ± 12 nm, further addition of the achiral precursor resulted in a significantly larger pitch, e.g., the pitch of the (20% **1S** + 80% **1A**) mixture has a pitch ***p*** of 604 ± 48 nm. These effects are further confirmed by CD spectroscopy showing a decrease in the intensity of the bisignate signals from 100% **1S** + 0% **1A** to 0% **1S** + 100% **1A** (Figure 2C).

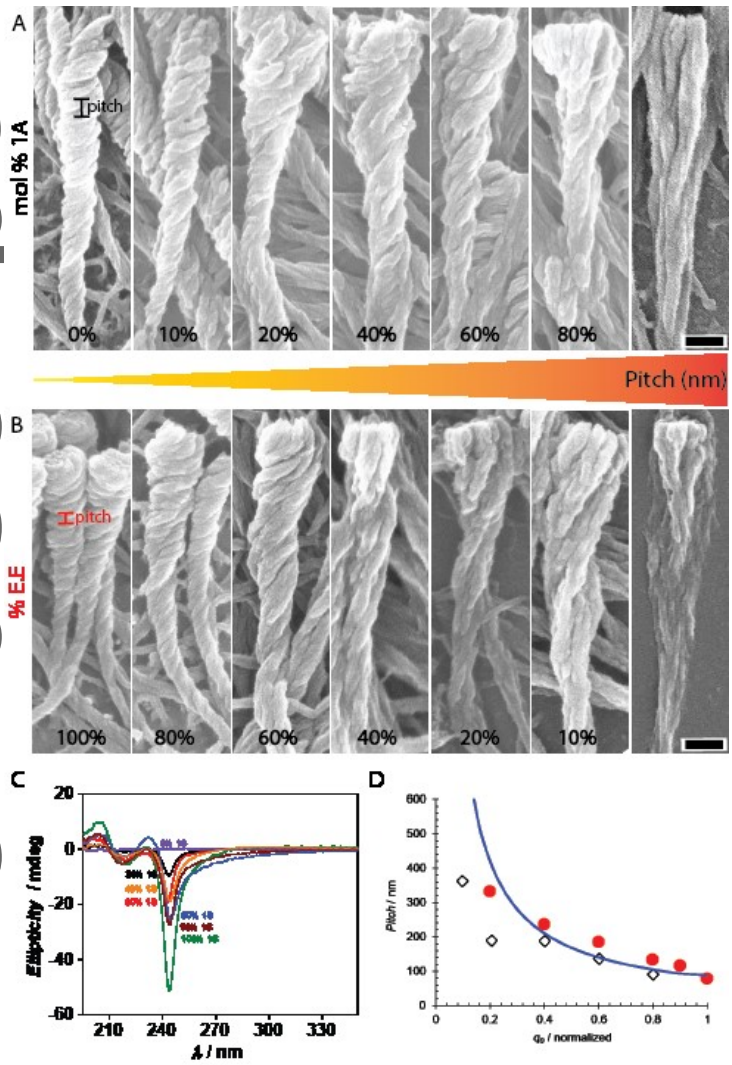

Figure 2. Enantiomeric purity of the molecular precursors defines the pitch of nanohelices during templated CVD polymerisation. (A) SEM images of representative polymer nanohelices prepared with varying amounts of 1S and 1A (1S + % 1A). Scale bar represents 200 nm. (B) SEM images of representative nanohelices prepared with varying amounts of 1S and 1R expressed as % E.E. Scale bar represents 200 nm. (C) CD spectra of the polymer nanohelices are shown in (A). (D) Pitches of nanohelices from experiments (red dots) and theoretical prediction (hollow diamonds) as a function of q_0; the blue line represents the computed pitch.

Similarly, the enantiomeric excess (E.E.) of the chiral precursors is a determining factor of the pitch observed in nanohelices (Figure 2B): Decreasing the E.E. of **1S** from 80 % to 10 % increased the average ***p*** value from 191 ± 21 nm to 743 ± 52 nm. Accordingly, the intensity of the signal at 242 nm in the

respective CD spectra (Figure S9, A) scaled proportionally to the E.E. of the precursor. Irrespective of the E.E. of the precursor used for templated CVD polymerisation, the IRRAS spectra were indistinguishable (Figure S9, B-C), suggesting that the composition of the respective nanohelices was identical. To better understand the mechanism of chiral transfer that results in the formation of enantiomorphically pure nanohelices, we placed our observations into the context of a simple model that considered the nanohelices and the LC as a single phase with a doubly-twisted director (***n***) configuration,[29] wherein the free energy associated with the orientational gradients can be expressed in terms of the Frank free energy:[30]

$$F = \frac{1}{2}\int dV[K_{11}(\nabla \cdot n)^2 + K_{22}((n \cdot \nabla \times n)^2 + q_o) + K_{33}(n \times \nabla \times n)^2 - 2K_{24}\nabla \cdot (n(\nabla . n) + n \times \nabla \times n)] \quad (2)$$

where K_{11}, K_{22} , K_{33} and K_{24} are the Frank elastic constants associated with splay, twist, bend, and saddle-splay deformations, and q_o is the twisting strength. As described previously,[29] minimization of the free energy of this model leads to the prediction that the pitch, ***p,*** changes with the twisting strength q_o as:

$$\boldsymbol{p} = \frac{8\pi(K_{24}-K_{22})}{3q_0K_{22}} \quad (3)$$

We characterise the twisting strength as q_o = x for (**1S** + **1A**) mixtures, where x= mole fraction of **1S**, and q_o = x – (1-x) = 2x-1; for (**1S** + **1R**) mixtures.[31] We assume commonly reported values of K_{22} (~ 10 pN) and K_{24} (~ 1.2 K_{22}) for the combined system comprised of polymer nanohelices and the LC phase,[32] the calculated pitches monotonically decrease with q_0. This prediction is consistent with our experimental observations **(**Figure 2D**)** and supports our conclusion that the chiral strength of the stereogenic center determines the pitch of the nanohelices.

2.2.2. Higher order arrangement of the nanohelices

Next, we considered higher-order arrangements of **2S** and **2R** nanohelices in the form of microscopic surface arrays (**Figure 3**, A-F). Dependent on their respective precursor stereochemistry, enantiomorphically pure nanohelices consistently resulted in microscopic clockwise (**2R**) or counter-clockwise (**2S**) patterns and appeared independent of the drying method. In contrast, no helical patterns are observed in arrays of achiral nanofibers (**2A**), evidently due to the achiral nature of **2A**. Corroborating this observation, the PLM images of nanohelices **2S** and **2R** after templated CVD

polymerisation, but prior to removal of the LC phase, also indicate the emergence of characteristic twist patterns (Figure 3, C and F). While qualitatively similar, nanohelices **2S** exhibited a larger twist (Figure 3, A-C) than nanohelices **2R** (Figure 3, D-F), which was attributed to differences in their respective enantiomeric purities of 99% E.E. (**1S**) and 97% E.E. (**1R**), a trend also visible in their corresponding POM images. Although a visible twist of the LC at the air interface is seen (Figure 3, C, F), it does not reveal signs of the typical fingerprint textures observed in cholesteric LC phases doped with small molecules of high, twisting powers.[33,34] This was further corroborated by the non-twisted patterns of both the nanohelices and that of the LC when a racemic precursor mixture **1S**+**1R** (1:1) was polymerised into the achiral E7 (Figure 3, G-I).

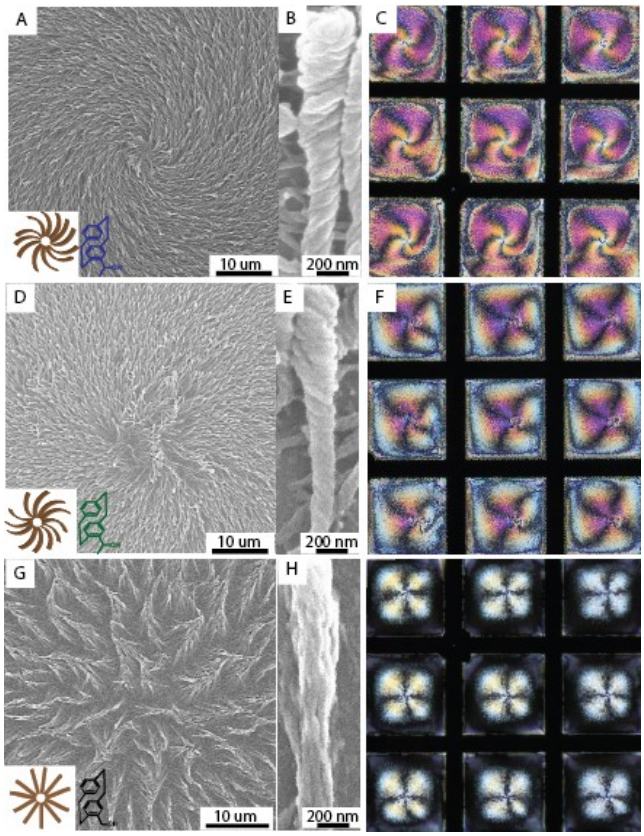

Figure 3. Large-area chirality in arrays of enantiomorphic nanohelices. (A-F) SEM images of nanohelices display counter-clockwise (2S, A, B) or clockwise (2R, D, E) patterns. The corresponding POM images of LC phases after CVD polymerisation. Inset shows a schematic of the nanofiber mesoscale structures and the monomer chemical structures. (G-H) SEM images of polymer nanofibers prepared from 1S with a 0% E.E (G, H). (I) The corresponding POM images representing the LC phases after CVD polymerisation.

The solid-state CD spectra of the nanohelices show broad bands at 275-339 nm and 340-700 nm both for **2S** (Figure S10, blue line) and **2R** (Figure S10, green line), but of opposite handedness due to their chiral nature and baseline signal in the case of racemic precursors (Figure S10, black line). As the additional broadbands are only observed for surface-supported nanohelices but not for nanohelices after removal from the substrate, we consider these bands a cooperative property of the mesoscale assemblies that emerges from the original molecular chirality of the precursors through superhierarchical chirality transfer, a phenomenon often observed in nature.[35] To further elucidate this effect, nanohelices with variable E.E. from 100 to 10% **1S** were prepared. For an E.E. above 80% (Figure S11), superhierarchical assemblies of enantiomorphic nanohelices were exquisitely controlled by the chiral purity of the precursor used for templated CVD polymerisation. In contrast, we observed loss of the counter-clockwise twist for nanohelices with decreasing E.E.

2.3. Competing chirality effects

So far, the role of molecular chirality of the precursor during templated CVD polymerisation has been the main focus of our investigations, and thus, achiral LC phases were employed. It is however worthwhile to explore how competing chiral information from the precursor and the templating LC phase may influence the formation of nanohelices. Replacing the nematic E7 phase with a cholesteric phase resulted in nanohelices displaying composite features that can be attributed to the chiral precursor (e.g., closed-looped pitch) and the templating cholesteric phase (e.g., curved fiber shape, **Figure 4**).

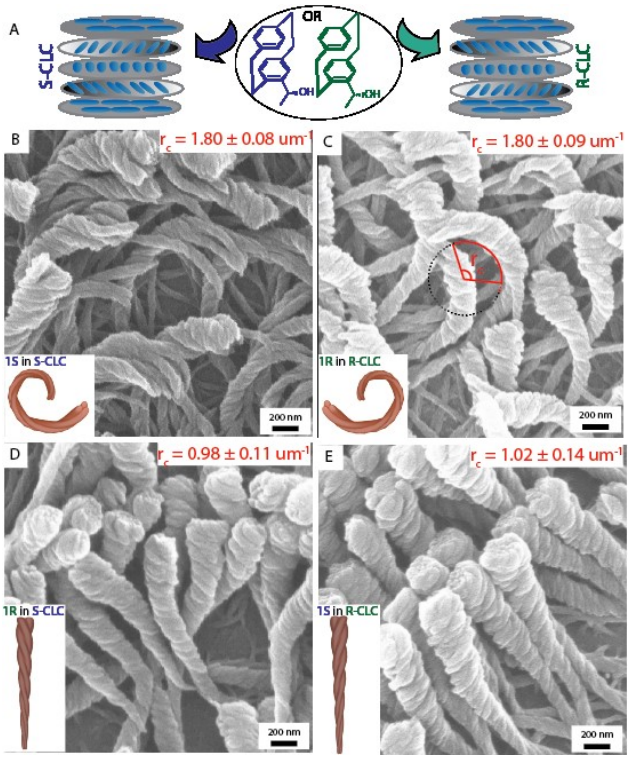

Figure 4. Templated synthesis of nanohelices using cholesteric LCs. (A) Schematic representation of templated CVD polymerisation of precursors 1S and 1R into S- (E7 doped with 2.4 wt-% S-811) and R-configured (E7 doped with 2.3 wt-% R-811) LC phases. (Left) SEM of polymer 2S (B) and 2R (D) templated by the S-CLC phase. (Right) SEM of polymer 2R (C) and 2S (E) templated by the R-CLC phase.

SEM images of nanohelices obtained by templated CVD polymerisation of the chiral precursors **1S** and **1R** into cholesteric LC phases comprised of E7 and 2.4 wt-% of either S- or R-811 dopants reveal nanohelices that resembled the nanohelices formed in an achiral E7 phase with regards to their tight pitches, but, additionally, displayed clockwise or counter -clockwise bends with a radius of curvature of 1.80 μm^{-1} (Figure 4, B-C and lower magnification images in Figure S12, A-B). In the case of the nanohelices shown in Figure 4B, the chiral information encoded in the precursor (**1S**) and the LC phase (S-811) appear to "synergize" structurally to give rise to pronouncedly bent nanohelices with radii of curvature consistently exceeding those observed for nanofibers prepared from achiral precursors (E7 + 2.3% S/R811 = 0.062 μm^{-1}). Similar chiral complementarity was observed for the combination of **1R** with the R-811 doped LC phase (Figure 4C). In the case of competing for chiral information between the chiral precursor and the LC phase, i.e., **1S** polymerised into a R811-doped LC phase, the curving

effect was suppressed, and relatively straight nanohelices were observed that were morphologically indistinguishable from nanohelices templated by the achiral E7 phase (Figure 4, D-E and lower magnification images in Figure S12, C-D). A similar "antagonistic" effect was observed for the combination of **1R** and the S811-doped LC phase. In principle, the relative effects of the two chiral contributors could be merely a question of stoichiometry with the chiral precursor overpowering the contributions from the doped LC phase. Thus, the amount of the chiral dopants S811 and R811 was systematically increased from 1 to 9%, and the resulting LC phases were used as the template for the CVD polymerisation of **1S**. In the synergistic case, bent nanohelices were observed in all cases, and the radius of curvature monotonically increased with increasing amounts of dopant (Figure S13). Once the dopant concentration reached a threshold concentration of about 5%, multi-domain organizations appeared resembling typical fingerprint patterns previously observed in cholesteric LC phases (Figure S13, C-E). In the antagonistic case, i.e., templated CVD polymerisation of **1S** into the R811-doped E7 phases, the nanohelices appeared straight, the pitch of the nanohelices remained unaltered, and their radii of curvature were consistently close to zero (Figure S14). These findings suggest that chiral elements of the precursor and the templating LC phase combine into nanohelices that can display synergistic or antagonistic features over multiple length scales: (i) If the chiral elements of precursor and LC phase match (i.e., 1R & E7+R811 or 1S & E7+S811), we observe bent nanohelices where their nanoscale features are similar to what has been observed for the CVD polymerization into achiral nematic phases, while their microscopic structure matches that of the cholesteric phase. In the opposite case (i.e., 1S & E7+R811), the nanohelices still maintain their original nanoscale structure, but their microscopic bending is drastically suppressed.

2.4. Detection of weak chirality using surfaces decorated with nanohelices

Next, we investigated the potential of surfaces decorated with nanohelices for the detection and enhancement of chirality in a nematic LC such as E7 doped with a chiral dopant S-DMPE, a system that otherwise appears to be achiral by CD spectroscopy (Figure S15). When a drop of the same LC mixture E7+5% S-DMPE was cast on the chiral substrates decorated with **2R** and **2S** nanohelices, characteristic fingerprint textures with pitches 20.82 ± 0.20 µm and 12.39 ± 1.30 µm was detected by cross-polarized light microscopy (**Figure 5**). Two different phenomena of chiral interaction were observed: (i) the pitch in the LC mixture E7+S-DMPE was smaller with increasing amounts of the dopant concentration on both **2R** and **2S** nanohelical substrates (Figure S16), and (ii) the induced pitch was larger for the LC mixture on the chiral substrate with **2R** nanohelices compared to that on **2S** (Figure 5, B-C). The

detection of chirality was an effect of the chiral translation, and consequently, the chiral strength of the surface-patterned nanohelices. This was proven by the absence of distinguishable fingerprint textures of LC mixtures E7+S-DMPE when dropped on chiral **2S** and **2R** polymer films (Figure S17).

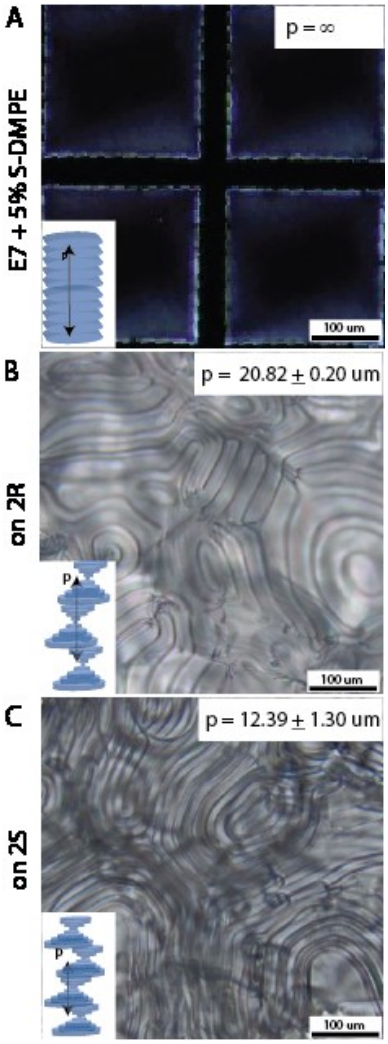

Figure 5. Chiral nanohelical assemblies as substrates for the detection of chirality in specific LC mixtures. E7 + S-DMPE that appears to be nematic (achiral) on a homeotropically anchored substrate (A) and by CD spectroscopy (Figure S15) shows a measurable pitch on surfaces decorated with 2R (B) and on 2S nanohelices (C). Insets provide a schematic representation of the twist in the LC mixture, i.e., their pitch on different substrates.

3. Conclusions

In summary, our results reveal that Nature's concept of multiscale chirality transfer can effectively inform the synthesis of enantiomorphic surfaces. Templated CVD polymerisation of precursor molecules with a single stereogenic center can result in enantiomorphically pure nanohelices where the E.E. defines the (i) contour length, (ii) pitch, (iii) twist angle, and (iv) mesoscale morphology of the nanohelices. Furthermore, these surface-supported nanohelices were arranged into microscopic twist patterns that displayed the homochirality encoded in the original precursor. Utilizing the transfer of chirality across length scales, such as amplifying weak chiral signatures by surfaces decorated with nanohelices shown in this work, appears to be an effective pathway towards superhierarchical chiral materials. Concomitantly, these enantiomorphically pure surfaces may serve as model surfaces that will contribute to a deeper understanding of nature's way to create homochirality via multiscale chirality transfer.

4. Experimental section

Materials

Sulfuric acid (98%, VWR), Hydrogen peroxide (H_2O_2, 30%, VWR), Dimethyloctadecyl[3-(trimethoxysilyl)propyl]ammonium chloride (DMOAP, VWR), E7 (Merck Japan), (1S)-1-(2,5-dimethylphenyl)ethanol (S-DMPE) and (1R)-1-(2,5-dimethylphenyl)ethanol (R-DMPE) (95%, Sigma Aldrich), (R)-2-Octyl 4-[4-(hexyloxy)benzoyloxy]benzoate (R811, 97%, Sigma Aldrich), S-(+)-2-Octyl 4-(4-hexyloxybenzoyloxy)benzoate (S811, 95%, Sigma Aldrich,)Acetone (EMSURE ACS, VWR), and Ethanol (EMSURE ACS, VWR) were used as received. Menzel microscope slides (Haeberle, prewashed and polished, 76 mm x 26 mm x 1 mm) were cut into approx. 1cm x 1cm wafers to prepare the nanohelices on these substrates. TEM grids (Cu grids, 75 mesh, 3.05 mm diameter, Plano) were used as purchased. Quartz glass plate (20 mm diameter, Suprasil QS, Hellma Optik, Jena, Germany) was cleaned and pre-treated prior to usage for CD spectroscopy as described in the experimental section 2.3. The starting materials, solvents, and reagents for the synthesis of **1S/R/A** were purchased from *Carbosynth* ([2.2]Paracyclophane, ≥99%) and *Sigma Aldrich* (Dichloromethyl methyl ether, 98%; Lithium aluminum Hydride, 95%; Methyl lithium, 1.6 M in Et_2O; Titanium tetrachloride, ≥97%) and were used without further purification. For reactions, extractions, and chromatography, solvents of *p.a.* quality were purchased from *Fisher Scientific* or *Merck*. For moisture and/or air-sensitive reactions, anhydrous solvents were taken from a solvent purification system.

Instrumentation

X-ray photoelectron spectroscopy (XPS)

XPS measurements were performed using a K-Alpha+ XPS spectrometer (ThermoFisher Scientific, East Grinstead, UK). All samples were analyzed using a micro-focused, monochromated Al Kα X-ray source (4100 µm spot size). The kinetic energy of the electrons was measured by a 180° hemispherical energy analyzer operated in the constant analyzer energy mode (CAE) at 50 eV pass energy for elemental spectra. The K-Alpha+ charge compensation system was employed during analysis, using electrons of 8 eV energy and low-energy argon ions to prevent any localised charge build-up. For data acquisition and processing, the Thermo Avantage software is used. The spectra were fitted with one or more Voigt profiles (BE uncertainty: ± 0.2eV), and Scofield sensitivity factors were applied for quantification.[36] All spectra were referenced to the C1s peak (C-C, C-H) at 285.0 eV binding energy.

Light microscopy

Polarised optical micrographs were obtained using an optical microscope (Olympus BX53) fitted with an LED light source, a polariser before the sample, and an analyzer after the sample. The polariser and analyser were positioned at 90 ° to each other to visualise the LC textures.

Scanning electron microscopy (SEM)

SEM images were taken using LEO 1530 Gemini scanning electron microscope (Zeiss, Germany) at the Institute of Nanotechnology (INT), KIT. Prior to taking SEM images, all samples were stuck onto conducting carbon tapes and glued to the stub using carbon glue thoroughly to create a layer of contact between the glass substrates and the carbon tape. Further, they were sputtered with approximately 6 nm of gold to prevent the charging of the polymeric fibers. All SEM images were measured at an electron accelerating voltage of 10 kV at a working distance of 2.5 mm.

Infrared reflection-absorption spectroscopy (IRRAS)

Surface-vibrational data of the fibers **2S, 2R,** and **2A** were recorded with a Bruker VERTEX 70 FT-IR spectrometer equipped with a Polarization Modulation Accessory (PMA) 50 unit (Bruker Optik GmbH, Ettlingen, Germany). The device was cooled with liquid nitrogen and equipped with an MCT detector and a horizontal reflection unit for grazing incidence (Bruker A518). A p-polarised beam at an incident angle of 80° to the surface normal was used for measurements. The spectra resolution of all recorded spectra is 4 cm^{-1}. The sample chamber was purged for a few minutes with dry nitrogen gas before and during all measurements.

IR spectra of the polymer precursors **1S, 1R,** and **1A** were recorded in an FT-IR Bruker IFS 88. The compounds were measured as pure substances by an ATR technique (ATR = attenuated total reflection). The position of the absorption band is given in wavenumbers ṽ in cm-1. The intensities of the bands were characterised as follows: vs = very strong (0–20% T), s = strong (21–40% T), m = medium (41–60% T), w = weak (61–80% T), vw = very weak (81 100% T).

Circular dichroism (CD) spectroscopy

CD measurements were performed both in solution and in solid-state (oriented CD). For the nanohelices dispersed in methanol, measurements were performed in a J-815 spectropolarimeter (JASCO, Gross-Umstadt, Germany) in quartz glass cells (Hellma, Muellheim, Germany) with a path length of 1 mm. The spectra were recorded between 195 and 350 nm. The following measurement parameters were used: data pitch (0.5 nm), scanning speed (20 nm min^{-1}), bandwidth (1 nm), and response (4 sec). Three measurements were taken for every sample, and the data were averaged over these measurements, including the subtraction of a spectrum of methanol as the baseline. All spectra were recorded at 25°C in a thermostat-controlled cell holder. The spectra were further processed with an adaptive smoothing algorithm incorporated in the JASCO analysis software.

Oriented CD (OCD) samples were prepared by growing the nanohelices **2S,2R,2A** on the quartz glass plate that served as a UV-transparent window in the OCD cell. The homemade setup used for the OCD measurements is described in detail by Buerck et al.[37] The solid-state oriented CD measurements were then carried out in a Jasco J-810 spectropolarimeter (Jasco, Tokyo, Japan). The quartz glass plate coated with DMOAP as the alignment agent was measured as a reference for the actual nanohelices as samples. OCD spectra were recorded between 700 nm and 195 nm at 8 different angles with 45 ° increments and averaged for each rotation angle. Three scans for each measurement at a scan rate of 10 nm min-1, 4 sec response time, and 1 nm bandwidth were recorded and averaged at every 45 ° rotation. The eight successive spectra were then averaged again and subtracted from the reference sample to obtain an accurate CD spectrum of the chiral twisted nanohelices.

Nuclear magnetic resonance (NMR) spectroscopy

The NMR spectra were recorded on the following NMR devices as solutions at room temperature:

^{1}H NMR 300 MHz and ^{13}C NMR 75 MHz: Bruker Advance 300

^{1}H NMR 400 MHz and ^{13}C NMR 101 MHz: Bruker Advance 400, Bruker Advance Neo 400

^{1}H NMR 500 MHz, ^{19}F NMR 471 MHz, and

^{13}C NMR 126 MHz: Bruker Advance III HD

Chemical shifts δ are expressed in parts per million (ppm) downfield from tetramethylsilane (TMS). References for ^{1}H NMR and ^{13}C NMR spectra were the residual solvent peaks of chloroform (^{1}H: δ = 7.26 ppm) and d1-chloroform (^{13}C: δ = 77.16 ppm), which was purchased from eurisotop. All coupling constants (J) are absolute values and are given in Hertz (Hz), whereby the indices indicate the number of bonds. The description of signals includes: s = singlet, d = doublet, t = triplet, q = quartet, quin = quintet, m = multiplet, dd = doublet of doublets and ddd = double doublet of doublets and so forth. The spectra were analyzed according to first order. The assignments of the signal structure in ^{1}H NMR spectra were made by the interpretation of the chemical shifts and the multiplicity and for ^{13}C NMR spectra by DEPT 135-spectra (DEPT = distortionless enhancement by polarization transfer) and are described as follows: + = primary or tertiary C-atom (positive DEPT-signal), – = secondary C-atom (negative DEPT-signal) and Cq = quaternary C-atom (no DEPT-signal) in combination with 2D NMR techniques such as COSY (Correlation Spectroscopy), HSQC (Heteronuclear Single-Quantum Correlation spectroscopy) and HMBC (Heteronuclear Multiple-Bond Correlation spectroscopy).

Mass spectrometry

Mass spectra were measured using EI (EI = electron impact) or FAB (FAB = fast atom bombardment) methods and recorded on a Finnigan MAT 95. For FAB measurements, 3-NBA (3 nitrobenzyl alcohol) was used as a matrix. ESI-MS (ESI = electron spray ionization) and ASAP-MS (ASAP = atmospheric pressure solids analysis probe) spectra were measured on a series Q Thermo Scientific mass spectrometer. The peaks are quoted as mass-to-charge-ratio (m/z) and the molecule peak is given as [M]+ or [M+H]+ (positive mode)/[M–H]+ (negative mode) and characteristic fragment peaks are given as [M–fragment]+ or [fragment]+. The signal intensities are given in percent relative to the intensity of the base signal (100%). For the high-resolution mass (HRMS), the following abbreviations were used: calcd. = calculated data, found = measured data.

Methods

Synthetic protocols for 1S, 1R, and 1A

General

(S_p)-4-Formyl[2.2]paracyclophane was prepared according to a literature procedure by Braun *et al*. and was obtained with an *ee* of 98% as determined by the NMR of the diastereomeric ratio of the starting material.[38]

Preparative work

All reactions were carried out under argon atmosphere in oven-dried glassware using standard Schlenk techniques. Liquids were transferred with plastic syringes and steel cannula, solids were added directly as powder. If not stated otherwise, the reactions were performed a room temperature (r.t.). For low temperatures, flat dewars with ice/water or isopropanol/dry ice mixture were used. The solvents were removed at 40 °C with a rotary evaporator under reduced pressure. For solvent mixtures, each solvent was measured volumetrically.

Purification: Thin-layer chromatography (TLC) and Column Chromatography

Analytical TLC was carried out on Merck silica gel coated aluminum plates (silica gel 60, F_{254}), detected under UV-light at 254 nm.

For flash column chromatography, silica gel 60 (0.040 × 0.063 mm, 230 –400 mesh ASTM) from *Merck* was used as stationary phase, and as mobile phase, solvents of p.a. quality were used.

Synthesis of (rac)-4-[2.2]Paracyclophanyl)methanol (1A)

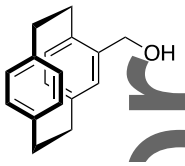

The compound was prepared according to a literature procedure by Delcourt *et al.* The spectroscopic data is in accordance with previous reports.[39,40]

^{1}H NMR (300 MHz, $CDCl_3$, ppm) δ = 6.61 (dd, J = 7.9, 1.9 Hz, 1H, H_{Ar}), 6.56 – 6.45 (m, 4H, H_{Ar}), 6.41 – 6.37 (m, 2H, H_{Ar}), 4.71 (dd, J = 12.8, 6.0 Hz, 1H, CH_2OH), 4.38 (dd, J = 12.8, 5.5 Hz, 1H, CH_2OH), 3.40 (ddd, J = 13.0, 10.0, 2.4 Hz, 1H, H_{PCP}), 3.19 – 2.96 (m, 6H, H_{PCP}), 2.87 (ddd, J = 13.3, 10.7, 5.8 Hz, 1H, H_{PCP}), 1.41 (t, J = 5.9 Hz, 1H, CH_2OH).

^{13}C NMR (126 MHz, $CDCl_3$, ppm) δ = 140.3 (C_q, C_{Ar}), 139.8 (C_q, C_{Ar}), 139.6 (C_q, C_{Ar}), 139.3 (C_q, C_{Ar}), 137.5 (C_q, C_{Ar}), 135.0 (+, CH, C_{Ar}), 133.4 (+, CH, C_{Ar}), 133.3 (+, CH, C_{Ar}), 132.4 (+, CH, C_{Ar}), 132.2 (+, CH, C_{Ar}), 132.1 (+, CH, C_{Ar}), 129.1 (+, CH, C_{Ar}), 64.5 (–, CH_2, CH$_2$OH), 35.3 (–, CH_2), 35.1 (–, CH_2), 34.4 (–, CH_2), 32.8 (–, CH_2).

Synthesis of (S_p,*S*)-1-(4-[2.2]Paracyclophanyl)ethanol (1S) and (S_p,*R*)-1-(4-[2.2]Paracyclophanyl)ethanol (1R)

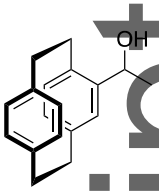

(S_p)-4-Formyl[2.2]paracyclophane (700 mg, 2.96 mmol, 1.00 equiv.) was dissolved in dry THF (22 mL) and cooled to –78 °C. Methyllithium (1.6 M in diethyl ether, 2.22 mL, 3.56 mmol, 1.20 equiv.) was slowly added, and the mixture was warmed to room temperature. After 16 h, ammonium chloride (sat. aq. solution, 20 mL) was added. The phases were separated, and the aqueous layer was extracted with ethyl acetate (3 x 20 mL). The combined organic layers were dried over sodium sulfate, and the solvent was removed under reduced pressure. After flash column chromatography (silica, *n*-pentane/EtOAc, 10:1) the title compound was obtained as separate diastereoisomers (S_p,*S* = ***1S***) (300 mg, 1.2 mmol, 56%) and (S_p,*R* = ***1R***) (115 mg, 456 µmol, 22%).

Fraction 1 (S_p,*S* = *1S*):

R_f = 0.34 (*n*-pentane/EtOAc, 4:1)

^{1}H NMR (500 MHz, $CDCl_3$, ppm) δ = 6.66–6.60 (m, 2H, H_{Ar}), 6.52 (qd, J = 7.8, 1.9 Hz, 2H, H_{Ar}), 6.47 (dt, J = 7.9, 2.4 Hz, 2H, H_{Ar}), 6.42 (d, J = 7.7 Hz, 1H, H_{Ar}), 4.95 (q, J = 6.4 Hz, 1H, C*H*CH_3), 3.34 (ddd, J = 13.7, 10.0, 2.1 Hz, 1H, H_{PCP}), 3.18 (ddd, J = 13.1, 10.7, 2.1 Hz, 1H, H_{PCP}), 3.14–3.02 (m, 5H, H_{PCP}), 2.84 (ddd, J = 13.7, 10.7, 6.2 Hz, 1H, H_{PCP}), 1.74 (s, 1H, CHO*H*), 1.30 (d, J = 6.4 Hz, 3H, CHCH_3).

^{13}C NMR (126 MHz, $CDCl_3$, ppm) δ = 144.9 (C_q, C_{Ar}), 140.5 (C_q, C_{Ar}), 139.8 (C_q, C_{Ar}), 139.5 (C_q, C_{Ar}), 135.2 (+, CH, C_{Ar}), 135.0 (C_q, C_{Ar}), 133.8 (+, CH, C_{Ar}), 133.2 (+, CH, C_{Ar}), 132.3 (+, CH, C_{Ar}), 131.7 (+, CH, C_{Ar}), 130.0 (+, CH, C_{Ar}), 128.3 (+, CH, C_{Ar}), 68.1 (+, CH, *C*HOH), 35.5 (–, CH_2), 35.4 (–, CH_2), 34.5 (–, CH_2), 33.3 (–, CH_2), 25.9 (+, CH_3, CH*C*H_3).

IR (ATR, cm^{-1}) $\tilde{\nu}$ = 3616 (s), 3608 (s), 3353 (s), 3337 (s), 3007 (w), 2968 (w), 2948 (m), 2924 (s), 2887 (w), 2847 (m), 1888 (vw), 1608 (w), 1591 (w), 1499 (w), 1448 (w), 1438 (w), 1414 (m), 1371 (w), 1320 (w), 1272 (w), 1225 (w), 1180 (w), 1145 (s), 1120 (s), 1060 (vs), 1024 (m), 963 (vw), 932 (w), 905 (s), 895 (m), 853 (s), 796 (m), 734 (w), 715 (s), 653 (s), 633 (s), 625 (s), 605 (vs), 575 (s), 558 (m), 533 (m), 521 (m), 504 (vs), 489 (s), 439 (w), 385 (w).

MS (FAB, 3-NBA, %) *m/z* = 252 (26) $[M]^+$, 235 (100) $[M–OH]^+$.

HRMS (FAB, $[M]^+$, $C_{18}H_{20}O$) calcd.: 252.1514; found: 252.1513.

Fraction 2 (S_p,*R* = *1R*):

R_f = 0.27 (*n*-pentane /EtOAc, 4:1)

^{1}H NMR (500 MHz, $CDCl_3$, ppm) δ = 6.56–6.47 (m, 5H, H_{Ar}), 6.39–6.34 (m, 2H, H_{Ar}), 4.87 (q, *J*=6.2, 1H, C*H*CH_3), 3.66 (ddd, *J*=13.6, 10.2, 2.4, 1H, H_{PCP}), 3.21–2.95 (m, 6H, H_{PCP}), 2.91 (ddd, *J*=13.6, 10.8, 5.8, 1H, H_{PCP}), 1.59 (d, *J*=6.5, 3H, CHCH_3), 1.33 (d, *J* = 5.8 Hz, 1H, CHO*H*).

^{13}C NMR (126 MHz, $CDCl_3$, ppm) δ = 142.4 (C_q, C_{Ar}), 140.4 (C_q, C_{Ar}), 139.7 (C_q, C_{Ar}), 139.6 (C_q, C_{Ar}), 138.7 (C_q, C_{Ar}), 135.8 (+, CH, C_{Ar}), 133.5 (+, CH, C_{Ar}), 133.2 (+, CH, C_{Ar}), 132.8 (+, CH, C_{Ar}), 132.1 (+, CH, C_{Ar}), 129.9 (+, CH, C_{Ar}), 129.8 (+, CH, C_{Ar}), 67.7 (+, CH, *C*HOH), 35.4 (–, CH_2), 35.3 (–, CH_2), 34.9 (–, CH_2), 33.5 (–, CH_2), 21.3 (+, CH_3, CH*C*H_3).

IR (ATR, cm^{-1}) $\tilde{\nu}$ = 3618 (w), 3322 (m), 3029 (w), 3007 (w), 2983 (w), 2968 (m), 2945 (m), 2922 (vs), 2888 (m), 2849 (m), 1884 (vw), 1592 (w), 1499 (w), 1485 (w), 1443 (w), 1411 (s), 1368 (s), 1320 (w), 1303 (w), 1289 (w), 1271 (w), 1242 (w), 1224 (w), 1204 (w), 1181 (w), 1146 (m), 1120 (w), 1077 (vs), 1060 (s), 1027 (s), 955 (w), 935 (m), 901 (m), 887 (s), 850 (vs), 793 (m), 756 (m), 734 (w), 714 (vs), 681 (w), 653 (vs), 608 (vs), 567 (w), 526 (m), 504 (vs), 484 (s), 460 (w), 443 (w), 439 (w), 422 (w), 384 (w).

MS (FAB, 3-NBA, %) *m/z* = 252 (28) $[M]^+$, 235 (100) $[M–OH]^+$.

HRMS (FAB, $[M]^+$, $C_{18}H_{20}O$) calcd.: 252.1514; found: 252.1514.

Preparation of nanohelices (2S, 2R) and 2A nanofibers

Preparation of substrates for the growth of nanohelices and nanofibers

Glass wafers of approximately 1 cm x 1 cm were cut using a diamond cutter and washed by immersing them into a bath of piranha (H_2SO_4:H_2O_2 = 3:1) solution and sonicating them for 20 min. They were then individually cleaned by dipping them into milliQ water followed by ethanol. The cleaned glass substrates were then coated with DMOAP to introduce homeotropic alignment in E7. For this, the piranha-washed and cleaned substrates were sonicated in DMOAP solution (2% in water in a beaker) after immersing them into the DMOAP solution for 15 minutes. They were then removed and washed individually with water followed by isopropanol and acetone to obtain uniformly coated glass substrates. This was verified by the clear, non-patchy appearance of the glass wafers. A. total of 2-4 TEM grids, depending on the dimensions of the substrate (typically a 1 cm x 1 cm wafer can accommodate 4 TEM grids), with a thickness of 10-12 µm were placed on every homeotropically aligned glass substrate. Lastly, 1 µL of the liquid crystal E7 was pipetted using a 0.1-10 µL micropipette

and carefully loaded onto the TEM grids until the liquid crystal formed a convex meniscus within the meshes of the grids. The meshes of the TEM grids that act as microwells for the liquid crystal are now overloaded. To obtain a flat film of LC with a uniform thickness, a capillary tube was used to carefully remove the excess liquid crystal in every TEM grid.

In the case of cholesteric LCs, the same procedure was followed for loading them into the TEM grids and removing the LC excess to obtain an even thickness of the film, except that they were loaded in their isotropic phase. A cleaned and homeotropically aligned glass substrate covered with the TEM grids was placed on a hot plate set to 70 °C (10 °C higher than the nematic-isotropic transition temperature of the nematic LC, E7 in this case as the nematic LC doped with the chiral dopant). After 1-2 minutes, when the glass wafer was hot, the CLC was carefully loaded onto the TEM grids using a 0.1-10 µL micropipette without touching the TEM grids, glass wafer, or the hot plate. As soon as the CLC is loaded, it turned transparent as it is in its isotropic phase. As described earlier, a capillary tube was used to carefully remove the excess CLC while on the hot plate to obtain a uniform thickness of the CLCs on the TEM grids. At this stage, the substrates were slowly cooled down to their nematic phase by turning off the hot plate and allowing it to cool down to room temperature under ambient conditions. The glass substrates with the TEM grids loaded with nematic or cholesteric liquid crystals were then ready for CVD polymerization. A similar procedure for cleaning, aligning the substrate, and loading the LCs into the TEM grids as described above on a glass substrate was performed on silicon, gold, and quartz substrates for XPS, IRRAS, and OCD measurements.

Growth of nanohelices and nanofibers by CVD polymerisation

4 mg of the monomer **1S**, **1R**, or **1A** was loaded into a quartz boat with a magnetic bar and placed at the far end of the CVD quartz tube from the furnace. The substrates loaded with LCs were placed in the deposition chamber where the stage was set to 15 °C (E7 exists in its nematic phase) and rotated at 30 rpm throughout the polymerisation process. The furnace was set to 550 °C in the central zone of a three-zone furnace. The other two zones were set to 560 °C and 500 °C, and the wall temperature around the deposition to 80 °C. Once the precursor and the substrates were placed in their respective chambers, the deposition chamber and the quartz tube were closed, and the entire system was evacuated. In about 10 minutes, when the vacuum reached a stable pressure of approximately 0.009 Torr, Argon was flushed through the end of the quartz tube at a constant rate of 20 sccm. When the

pressure again stabilised at approximately 0.130 Torr, the monomer boat was moved towards the furnace and placed at a distance of 3 cm from it. At this distance, the monomer begins to sublime, being placed at around 120 °C. As soon as the boat containing the monomer is placed at 3 cm distance from the furnace, the deposition controller is turned on, and the deposition of the monomer onto the substrates is monitored. A constant deposition rate of 0.2-0.4 Å/sec is maintained throughout the deposition process. When the readout is zero, the monomer boat is pulled back to its starting position. The argon supply is turned off, and the entire system is brought back to atmospheric pressure to enable the removal of the substrates from the deposition chamber.

Washing the nanohelices to remove LC

All substrates after CVD polymerisation were individually washed in acetone followed by ethanol for 3 minutes each. This cycle was repeated 3 times to ensure the complete removal of LC from the nanohelices and the substrate. During washing, the substrates were placed at 45° inside a glass vial containing the washing solvent and slowly shaken on an orbital shaker.

Drying the substrates to obtain dry nanohelices on the substrate

After performing the washing cycles ensuring the complete removal of the LCs from the substrates, the substrates were removed from the washing solution (acetone or ethanol) and placed on a flat surface. The substrates were air-dried for 2h to allow the residual solvents to evaporate at atmospheric pressure and room temperature. The obtained dry nanohelices on the substrates were then used for respective characterizations.

Supporting Information

Supporting Information is available from the Wiley Online Library or from the author.

Acknowledgements

This work has been in parts supported by the National Science Foundation through Grant 1916654 (J. Lahann, N. Abbott). Financial contributions from the German Research Foundation (formally Deutsche Forschungsgemeinschaft DFG) in the framework of SFB1176 Cooperative Research Centre "Molecular Structuring of Soft Matter" (CRC1176, C2) and the cluster “3D Matter Made To Order” funded under Germany’s Excellence Strategy -2082/1--390761711 are greatly acknowledged (all S. Braese).

Received: ((will be filled in by the editorial staff))
Revised: ((will be filled in by the editorial staff))
Published online: ((will be filled in by the editorial staff))

References

[1] X. Feng, V. Marcon, W. Pisula, M. R. Hansen, J. Kirkpatrick, F. Grozema, D. Andrienko, K. Kremer, K. Müllen, *Nat. Mater.* **2009**, *8*, 421.

[2] Y. Yan, R. Wang, X. Qiu, Z. Wei, *J. Am. Chem. Soc.* **2010**, *132*, 12006.

[3] Y. Zhang, P. Chen, L. Jiang, W. Hu, M. Liu, *J. Am. Chem. Soc.* **2009**, *131*, 2756.

[4] T. Tu, W. Fang, X. Bao, X. Li, K. H. Dötz, *Angew. Chemie Int. Ed.* **2011**, *50*, 6601.

[5] W. Zou, Y. Yan, J. Fang, Y. Yang, J. Liang, K. Deng, J. Yao, Z. Wei, *J. Am. Chem. Soc.* **2014**, *136*, 578.

[6] G.-F. Liu, D. Zhang, C.-L. Feng, *Angew. Chemie Int. Ed.* **2014**, *53*, 7789.

[7] P. Ringler, W. Müller, H. Ringsdorf, A. Brisson, *Chem. – A Eur. J.* **1997**, *3*, 620.

[8] E. M. Wilson-Kubalek, R. E. Brown, H. Celia, R. A. Milligan, *Proc. Natl. Acad. Sci.* **1998**, *95*, 8040 LP.

[9] G. M. Whitesides, M. Boncheva, *Proc. Natl. Acad. Sci.* **2002**, *99*, 4769 LP.

[10] G. Huang, Y. Mei, *J. Mater.* **2015**, *1*, 296.

[11] J. K. Gansel, M. Thiel, M. S. Rill, M. Decker, K. Bade, V. Saile, G. von Freymann, S. Linden, M. Wegener, *Science (80-.).* **2009**, *325*, 1513 LP.

[12] M. Thiel, M. Decker, M. Deubel, M. Wegener, S. Linden, G. von Freymann, *Adv. Mater.* **2007**, *19*, 207.

[13] Z. Yang, M. Zhao, P. Lu, *Opt. Express* **2011**, *19*, 4255.

[14] M. Esposito, V. Tasco, M. Cuscunà, F. Todisco, A. Benedetti, I. Tarantini, M. De Giorgi, D. Sanvitto, A. Passaseo, *ACS Photonics* **2015**, *2*, 105.

[15] M. Esposito, V. Tasco, F. Todisco, A. Benedetti, D. Sanvitto, A. Passaseo, *Adv. Opt. Mater.* **2014**, *2*, 154.

[16] S. Matsui, in (Ed.: B. Bhushan), Springer Berlin Heidelberg, Berlin, Heidelberg, **2010**, pp. 211–

229.

[17] I. Utke, P. Hoffmann, J. Melngailis, *J. Vac. Sci. Technol. B Microelectron. Nanom. Struct.* **2008**, *26*, 1197.

[18] K. C. K. Cheng, M. A. Bedolla-Pantoja, Y.-K. Kim, J. V Gregory, F. Xie, A. de France, C. Hussal, K. Sun, N. L. Abbott, J. Lahann, *Science* **2018**, *362*, 804 LP.

[19] K. Akagi, G. Piao, S. Kaneko, K. Sakamaki, H. Shirakawa, M. Kyotani, *Science* **1998**, *282*, 1683 LP.

[20] H. Nandivada, H. Y Chen, J. Lahann, *Macromolecular Rapid Communications* **2005**, 26, 1794-1799.

[21] H.Y. Chen, J. Lahann, *Advanced Materials* **2007**, *19*, 3801-3808.

[22] X. Jiang, H.-Y. Chen, G. Galvan, M. Yoshida, J. Lahann, *Advanced Functional Materials* **2008**, *18*, 27-35.

[23] F. Xie, X. Deng, D. Kratzer, K. Chang, C. Friedmann, S. Qi, L. Solorio, J. Lahann, Angewandte Chemie Int. Ed. **2017**, 56, 203-207.

[24] M. Koenig, J. Lahann, Beilstein Journal of Nanotecchnology **2017**, 8, 2219-2220.

[25] W. Ye, Z. Li, R. Yuan, P. Zhang, T. Sun, M. Cai, X. Wang, J. Zhu, Y. Sun, H. Xing, *Liq. Cryst.* **2019**, *46*, 349.

[26] N. Berova, K. Nakanishi, R. W. Woody, *Circular Dichroism: Principles and Applications*, Wiley, **2000**.

[27] J. Lu, W. Gu, J. Wei, W. Zhang, Z. Zhang, Y. Yu, N. Zhou, X. Zhu, *J. Mater. Chem. C* **2016**, *4*, 9576.

[28] W.-R. Chen, J.-C. Hwang, *Liq. Cryst.* **2004**, *31*, 1539.

[29] G. M. Grason, *Soft Matter* **2020**, *16*, 1102.

[30] K. Nayani, R. Chang, J. Fu, P. W. Ellis, A. Fernandez-Nieves, J. O. Park, M. Srinivasarao, *Nat. Commun.* **2015**, *6*, 8067.

[31] C. Peng, O. D. Lavrentovich, *Soft Matter* **2015**, *11*, 7257.

[32] E. Pairam, J. Vallamkondu, V. Koning, B. C. van Zuiden, P. W. Ellis, M. A. Bates, V. Vitelli, A. Fernandez-Nieves, *Proc. Natl. Acad. Sci.* **2013**, *110*, 9295 LP.

[33] L. Wu, H. Sun, *Phys. Rev. E* **2019**, *100*, 22703.

[34] A. Wulf, *J. Chem. Phys.* **1974**, *60*, 3994.

[35] S. M. Morrow, A. J. Bissette, S. P. Fletcher, *Nat. Nanotechnol.* **2017**, *12*, 410.

[36] J. H. Scofield, *J. Electron Spectros. Relat. Phenomena* **1976**, *8*, 129.

[37] J. Bürck, S. Roth, P. Wadhwani, S. Afonin, N. Kanithasen, E. Strandberg, A. S. Ulrich, *Biophys. J.* **2008**, *95*, 3872.

[38] C. Braun, S. Bräse, L. L. Schafer, *European J. Org. Chem.* **2017**, *2017*, 1760.

[39] M.-L. Delcourt, S. Felder, S. Turcaud, C. H. Pollok, C. Merten, L. Micouin, E. Benedetti, *J. Org. Chem.* **2019**, *84*, 5369.

[40] S. Sugiyama, Y. Aoki, K. Ishii, *Tetrahedron: Asymmetry* **2006**, *17*, 2847.

Table of contents

We describe a liquid crystal templated approach to prepare nanohelices of chiral parylene polymers on surfaces with tunable length, pitch, and higher-order mesoscale morphologies by altering the chirality of the template and/or the precursor. A phenomenon of chirality transfer from molecular to mesoscale level takes places during chemical vapor deposition, allowing for detection of weak chiral signals on such surfaces.

Divya Varadharajan, Karthik Nayani, Christoph Zippel, Eduard Spuling, Kenneth C. Cheng, Swetha Sarangarajan, Sangchul Roh, Vanessa Trouillet, Stefan Bräse, Nicholas L. Abbott*, Joerg Lahann*

Surfaces decorated with enantiomorphically pure polymer nanohelices via hierarchical chirality transfer across multiple length scales